Domain wall trajectory determined by its fractional topological edge defects

Topological Edge Defects

Aakash Pushp[1][*][§], Timothy Phung[1, 2][*], Charles Rettner[1], Brian P. Hughes[1], See-Hun Yang[1], Luc Thomas[1], Stuart S.P. Parkin[1][§]

[1]IBM Almaden Research Center, San Jose, California 95120, USA

[2]Department of Electrical Engineering, Stanford University, Stanford, California 94305, USA

I. The topological theory of defects applied to magnetic domain walls

An ordered medium such as a ferromagnet can be regarded as a region of space that can be described by a function that assigns to every point of the region an order parameter[1,2]. For 2 dimensional ferromagnetic thin films, as in our case, typically the order parameter is taken as a unit vector of magnetization constrained to lie in the plane of the film. The order parameter space can therefore be taken as the circumference of a circle, which we will call the θ-space, where θ is defined as the angle that the magnetization makes to a fixed direction, say the x-axis, in the film. As the magnetization is continuous, it can be mapped onto the circumference of the circle, i.e., the θ-space. In a non-uniform media the order parameter varies continuously except at a singularity, known as a defect, where the order parameter is ill defined. The presence of a topological defect can be observed infinitely far away in terms of the winding number, n, associated with the order parameter as one

traverses around the singularity in a real system. In our case, it is the total angle θ that gets traversed when mapping the magnetization vector with respect to the x-axis while completing a loop of any shape around the defect. As the order-parameter space is a circle, the total angle traversed has to be a multiple of 2π. The winding number, n, is thus the number of times the θ-space gets traversed by 2π while going around a defect.

In simple magnetic systems and for the purposes of describing domain walls in this paper, the defects at the boundaries or in the bulk can be associated with the following winding numbers or their derivatives[3].
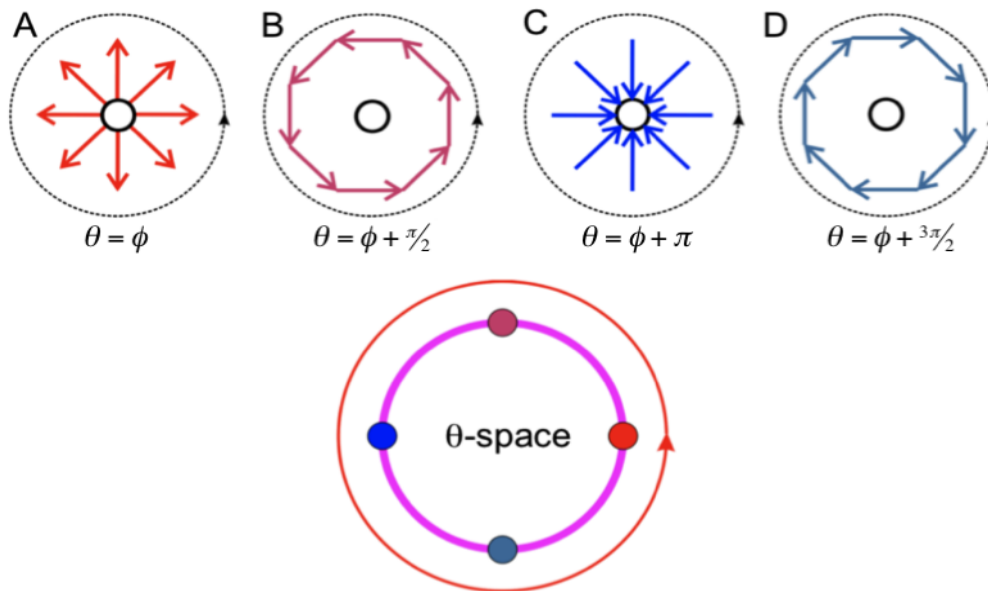

Figure S1 (A to **D)** Different magnetization configurations for n = +1. Pink circle indicates the order parameter space. For counter clockwise (CCW) traversal (dashed black curve) in the real space, θ also traverses in the CCW direction (shown by red curve) to map the magnetization angle with the chosen x-axis. Full circles indicated on the pink circle correspond to the offsets for the magnetization curves of the same color.

Fig. S1 shows defects with different magnetization profiles with a winding number of +1 because as one loops around them, say in counter clockwise (CCW) direction, as indicated by dashed black lines while mapping the magnetization onto the θ-space, the angle θ also completes one full circle in the same CCW direction as indicated by the arrow on the red circle. The initial phase shift differentiates the different magnetization profiles shown in Fig. S1 even though their winding number is the same. Although CCW and clockwise (CW) magnetization have opposite chiralities as shown in Fig. S1 B and D respectively, they have the same n = +1. In the following example, one needs to rotate in the opposite direction in the θ-space with respect to the direction of rotation in the real space in order to map the magnetization vector onto the θ-space.
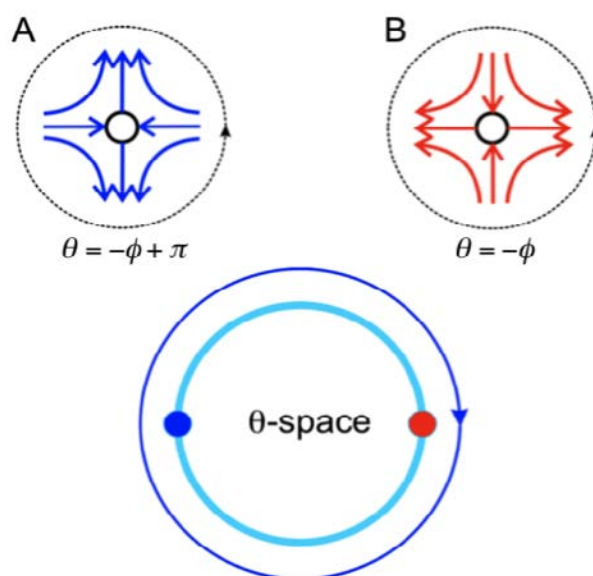

Figure S2 (A and **B)** Different magnetization configurations for n = -1. Cyan circle indicates the order parameter space. For CCW traversal (dashed black curve) in the real space, θ traverses in the opposite (CW) direction (shown by blue curve) to map the magnetization angle with the chosen x-

axis. Full circles indicated on the cyan circle correspond to the offsets for the magnetization curves of the same color.

The concept of using topological defects with n = ±1 and n = ±½ for describing the magnetic texture of DWs in a magnetic NW was first introduced by Tchernyshyov *et al* [3] by drawing analogy to the XY model. They pointed out that to describe the magnetic profile around a defect in the bulk of the ferromagnetic NW the solutions must be that of the Laplace equation with integer winding numbers, whereas the solutions at the edges can be obtained by the well-established method of images in the XY – model for electrostatic charges[2] and could be described by n = ±½.

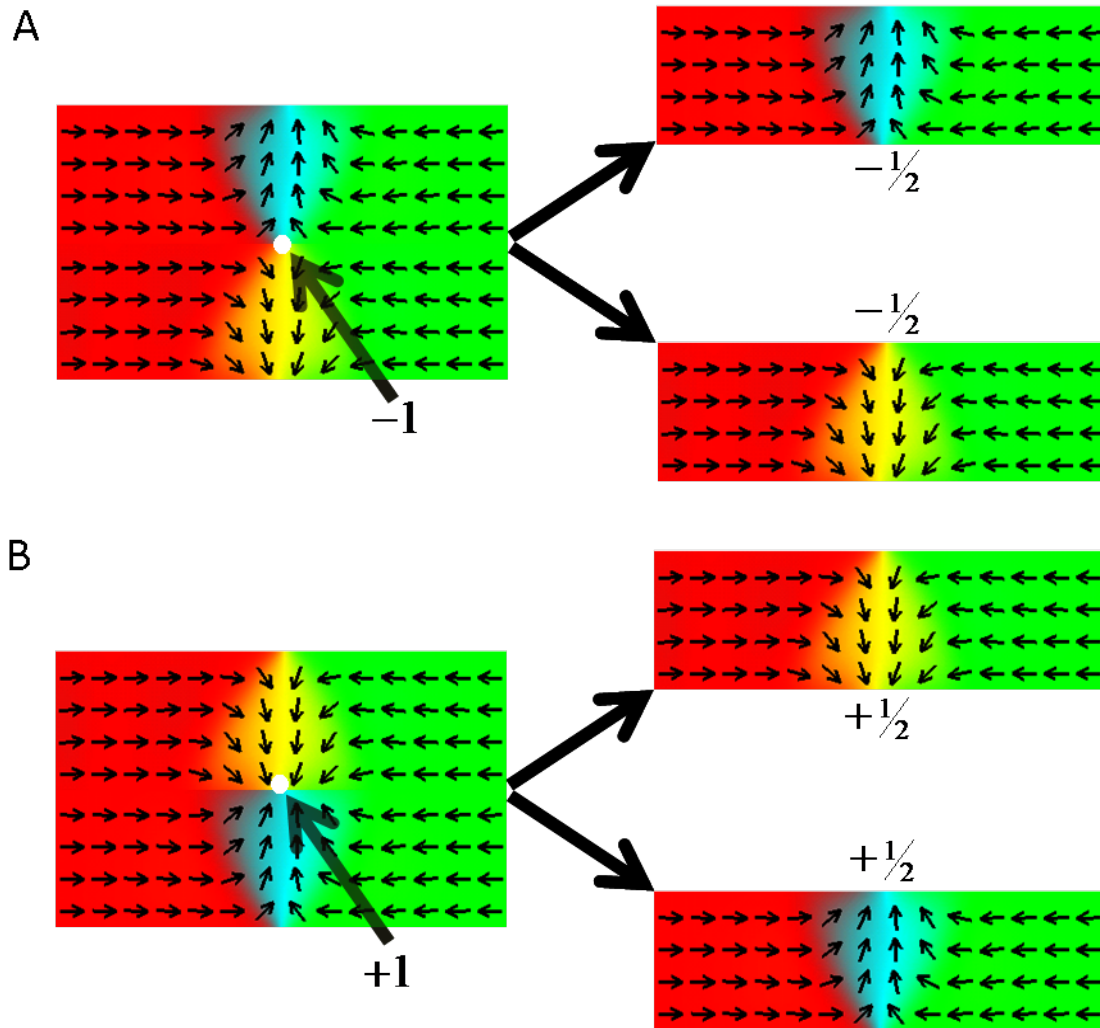Intuitively, one can visualize the winding number of the edge defects as shown in the following Fig. S3.

Figure S3 (A and **B)** Intuitively n = -1 and n = +1 defects can be split in half to give the respective n = -½ and n = +½ defects on the edges of transverse DWs.

With the integer as well as fractional winding numbers defined above, one can easily associate them with different DWs in terms of topological defects. We will consider head to head (HH) DWs here. Tail to tail (TT) DWs picture can be obtained by their time-reversed counterparts, i.e., flipping the magnetization arrows by π. So, CCW HH is equivalent to CW TT, etc.
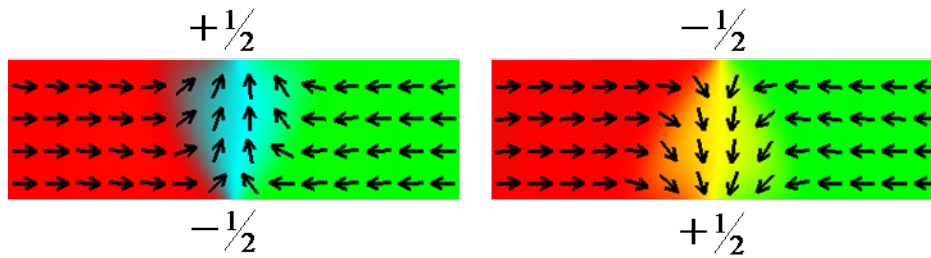
Figure S4 Transverse Walls CCW HH (left) and CW HH (right) consist of two defects indicated by their winding numbers: seen in narrower NWs.
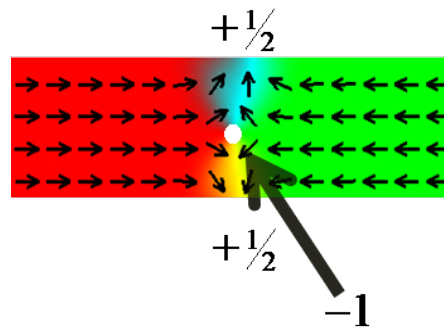

Figure S5 Anti-vortex Wall seen in narrower NWs consists of two $+\frac{1}{2}$ and one -1 defects. Unstable: only seen in transient states under magnetic field above Walker breakdown.
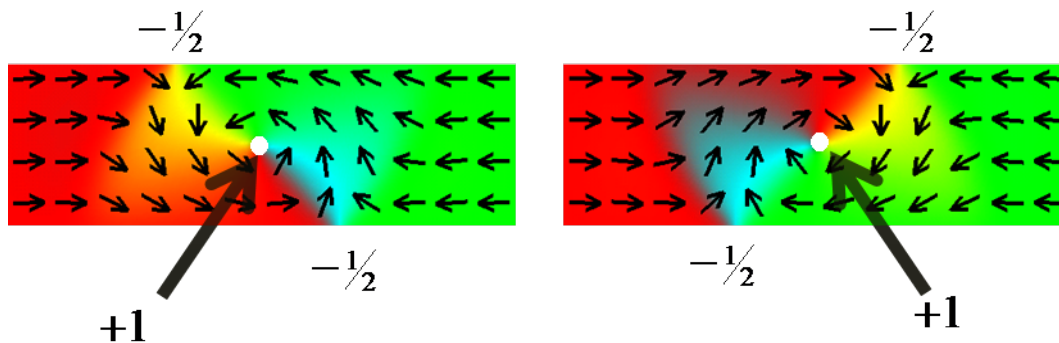

Figure S6 Vortex Walls- CCW (left) and CW HH (right) consist of two $-\frac{1}{2}$ and one +1 defects: seen in wider NWs.

More importantly, Tchernyshyov *et al.* [3] also pointed out that the defects with fractional winding numbers can only exist at the edges of the NW. Existence of an n = ±½ defect in the bulk would require a series of magnetic charges along a line connecting the defect to the edge, which is energetically unfavorable. The only way a

+½ (-½) winding number defect can move into the bulk of the NW is by switching to

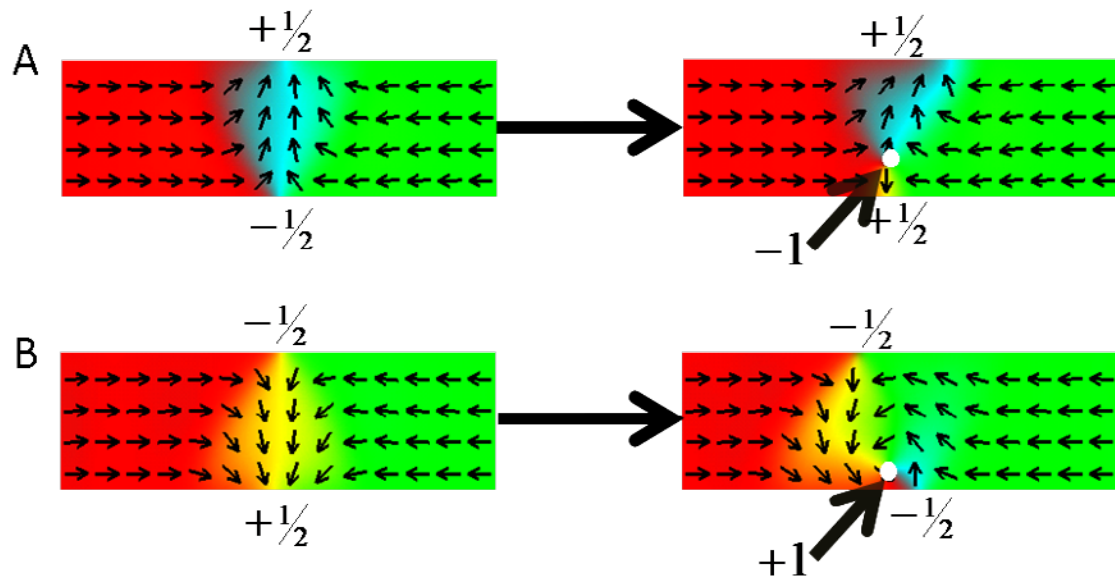a +1 (-1) winding number defect while leaving -½ (+½) on the edge as shown below.

'

Figure S7 (A and B) Above Walker breakdown, a transverse DW has two ways of injecting an n = +1

or n = -1 defect in the middle of the NW.

This is precisely the picture for a transverse DW moving in a NW above the

Walker breakdown field[4], where it switches to the opposite chirality via a transient

vortex or anti-vortex DW.

In principle, +½ (-½) winding number defect could move into the bulk by

switching to a -1 (+1) winding number defect but the remnant n = +3/2 (-3/2)

defect (as n has to be conserved) at the edge will cost a large exchange energy due to

a much higher curvature in magnetization.

II. Chirality conservation in a vortex domain wall

Vortex DWs are energetically favored over transverse DWs in wider NWs[5]. Above the Walker breakdown, a vortex DW traverses the NW by switching its polarity by going through an asymmetric transient transverse DW state (Fig. S8).
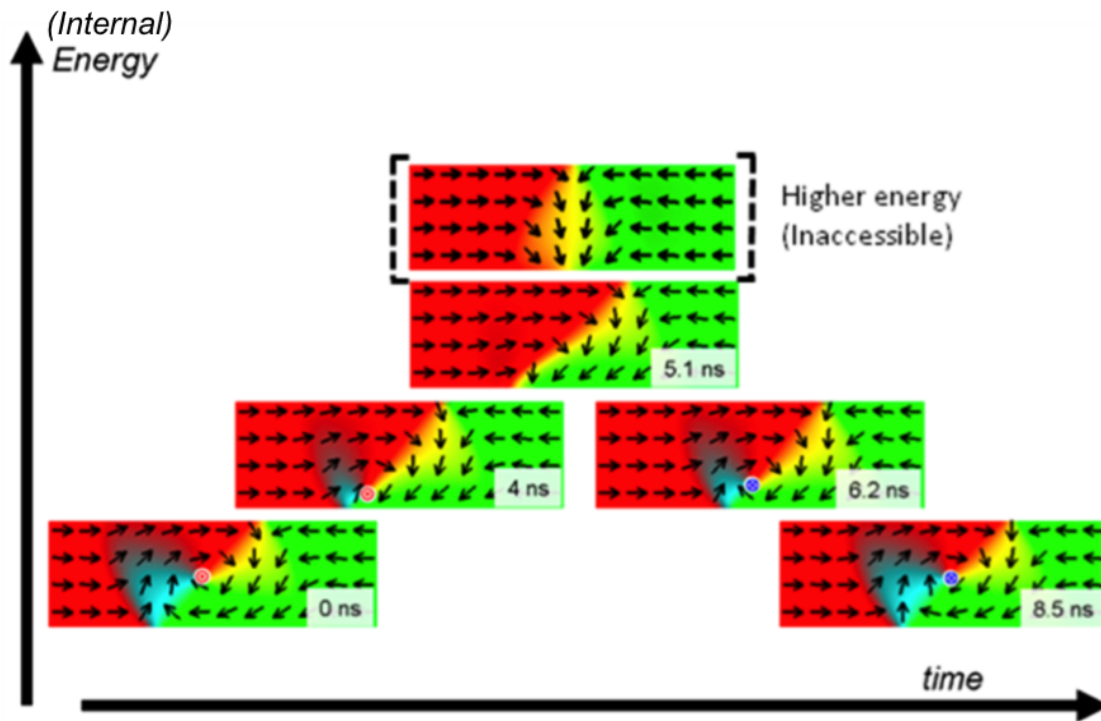

Figure S8 As a function of time, the CW HH DW switches its polarity while preserving its chirality. In doing so, it goes through a transient asymmetric transverse DW structure, which is lower in energy than the symmetric transverse DW due to the Zeeman energy. The magnetic field points in the positive x direction, which moves the up pointing polarity towards the bottom edge due to gyrotropic force[6].

This happens above the Walker breakdown when its vortex core with n = +1 defect, depending on its polarity and magnetic field direction, merges with one of the edge (n = -½) defects[7,8]. If, however, the vortex DW could go through a

symmetric transverse state that changed its symmetry to the opposite kind before ejecting out a vortex of the opposite polarity, it could switch its chirality as well. This is energetically unfavorable because of the Zeeman energy, which is driving the DW above Walker breakdown in the first place, that keeps the DW distorted during the polarity switching. Also, polarity switching, depending on the magnitude of the magnetic field, happens on rather fast time scales, during which the asymmetric DW doesn't have enough time to switch its symmetry. This way the core re-forms from where it had merged with the n=-½ defect with opposite polarity[8]. For larger cross-sectional area, the vortex DW state is energetically more favorable than the transverse DW, which makes chirality conservation even more robust.

III. Details of the domain wall injection process

At the minimum injection field, H^c, required for DW nucleation, vortex cores of a magnetic DW should nucleate from the weakest location along the NW, i.e., in the case of a perfect NW with no edge defects or inhomogeneities, the magnetic moments near an edge of the NW will be the first to flip because of the lower exchange energy. It would require twice the amount of exchange energy to flip the magnetic moment in the bulk of the NW.
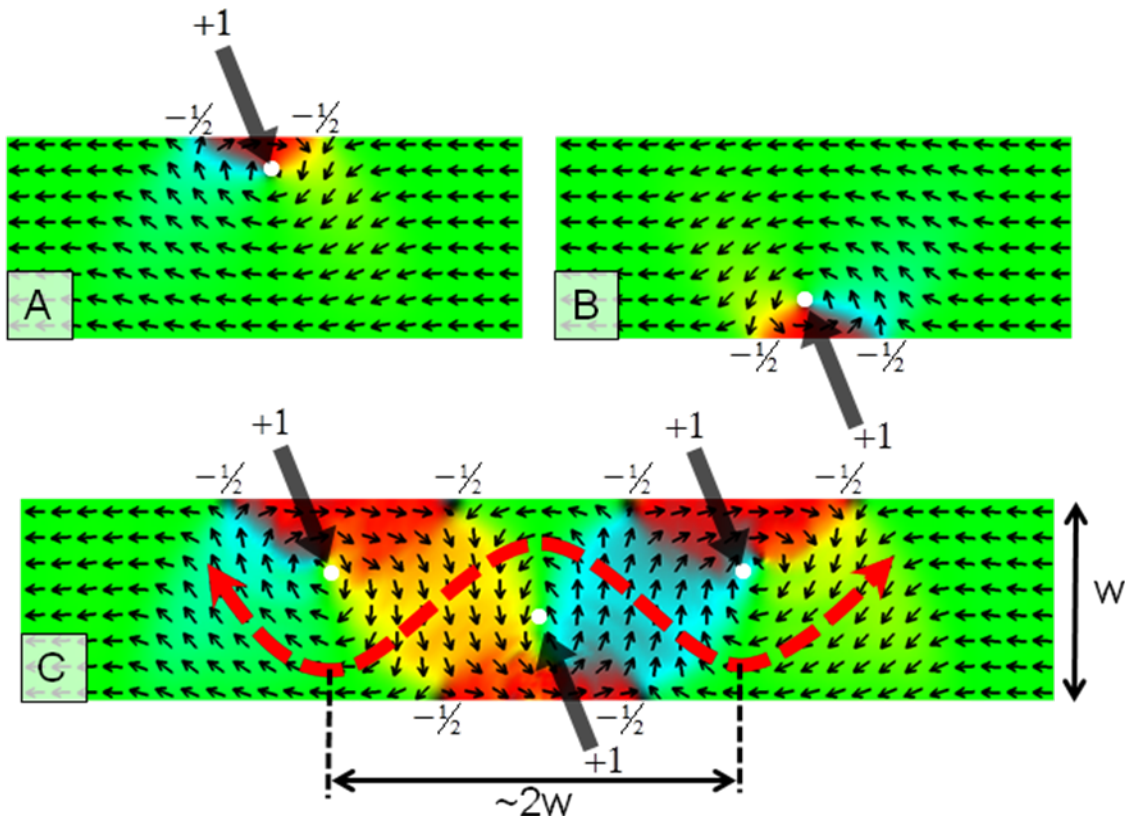

Figure S9 (A and B) For a NW magnetized in −x direction, if the domain reversal starts from top (bottom) edge, the core will be CW (CCW). **(C)** At higher fields oscillatory buckling of the magnetization leads to formation of multiple cores whose chirality depends on the edge at which they originate.

The key to chirality control of the injected DWs then stems from the observation that the chirality of the DW gets decided by the edge of the NW where the core of the DW originates. At all times, the sum of winding numbers of the various defects that form during domain reversal and growth has to stay preserved. So, for the NW of the dimensions in our measurements, a bulk defect with n=+1 that eventually forms the core of a DW, always gets created with two n=-½ defects originating from the same edge of the NW as shown in Fig S9, followed by creation of intermediate states (see Fig. 2c and movie S1) composed of a vortex and an anti-vortex pair. When a vortex and an anti-vortex core are created during the domain wall formation, they always have opposite polarities so as to conserve the net Skyrmion number[9]. This clearly locks the chirality of the bulk defect depending on whether the defect formation started on the top or bottom edge. At higher fields, the magnetization in the NW initially buckles in a sinusoidal fashion with a period close to twice the width of the NW (Fig. S9C). Eventually, the magnetization obtains a component perpendicular to the plane of the NW (see Movies S1 and S2), from where the cores originate, with their chirality decided by which edge they originated from in the NW. By engineering a defect in the shape of a notch on, say, the bottom edge (Fig. 2B), we merely reduce H^c required for domain reversal for that edge thereby biasing one edge over the other and thus favoring one chirality over another at the minimum required field for DW injection. Due to the oscillatory buckling of the magnetization for higher fields, cores also emanate from the opposite edge and thus are of the opposite chirality. As these cores are further along

the NW, they eventually are the ones that get inserted into the main section of the NW as discussed in the main text.

In order to further clarify the picture, a blow-up of the micromagnetic simulations shown in Fig. 2C and 2D is shown in Figs. S10 and S11 respectively. Also indicated are the vortex cores along with their polarities and type. The domain wall injection process occurs under rather large magnetic fields. Consequently, it entails the formation and annihilation of multiple topological defects, which is difficult to keep track. In order to simplify our understanding, the legends shown below define the symbols used to denote each core. The non-dominant cores appear only during the transient process of injecting the DW and are not part of the final DWs that are injected into the nanowire. We note that the anti-vortex cores are always non-dominant.

⊙ + dominant vortex core
⊗ - dominant vortex core
● + non-dominant vortex core
✕ - non-dominant vortex core
✚ + anti-vortex core
✚ - anti-vortex core

Figure S10 Blow up of the micromagnetic simulations from Fig. 2C showing the injection process for 51 mA of current applied to the injection line, resulting in the formation of CCW DWs injected into the nanowire.
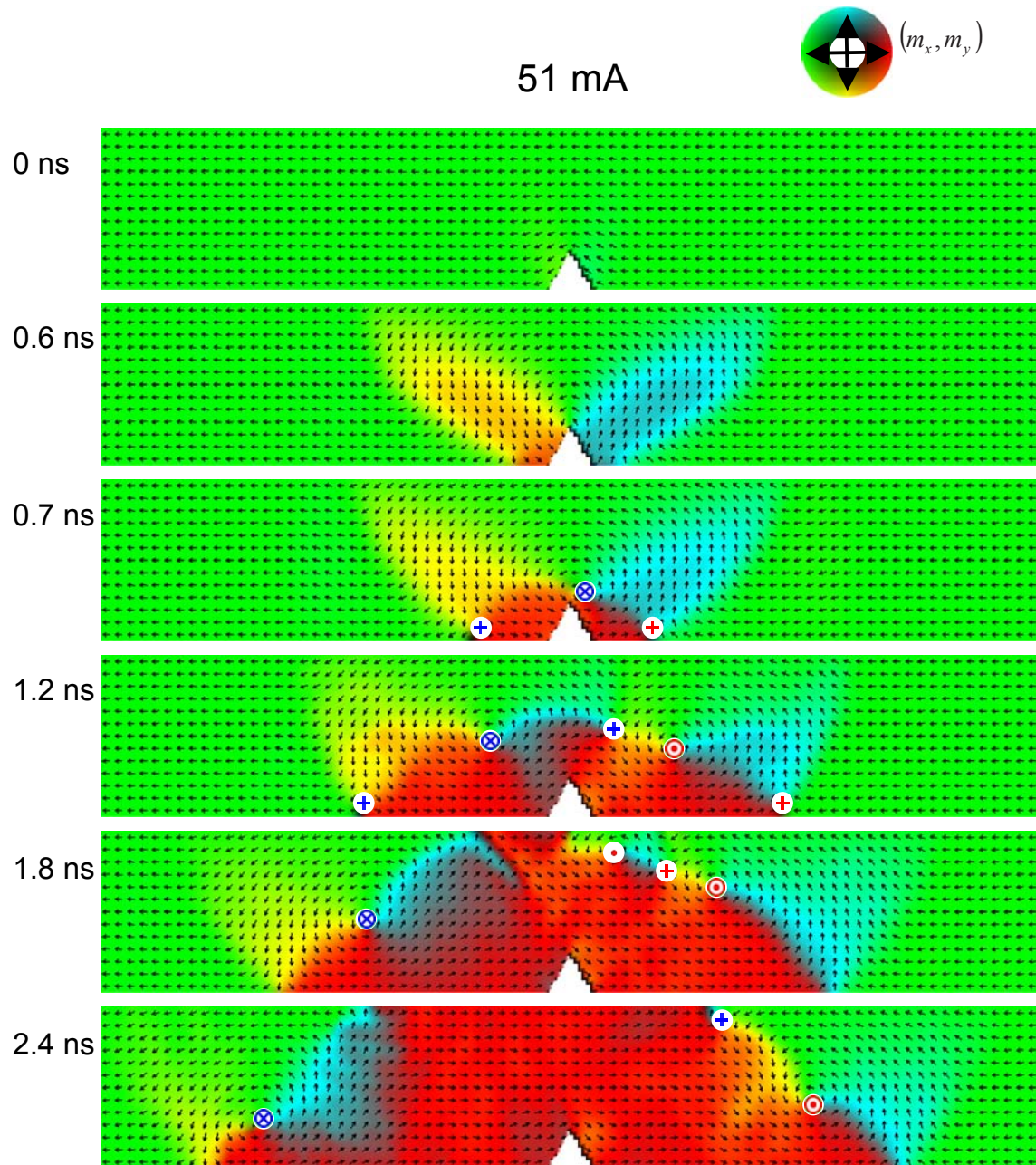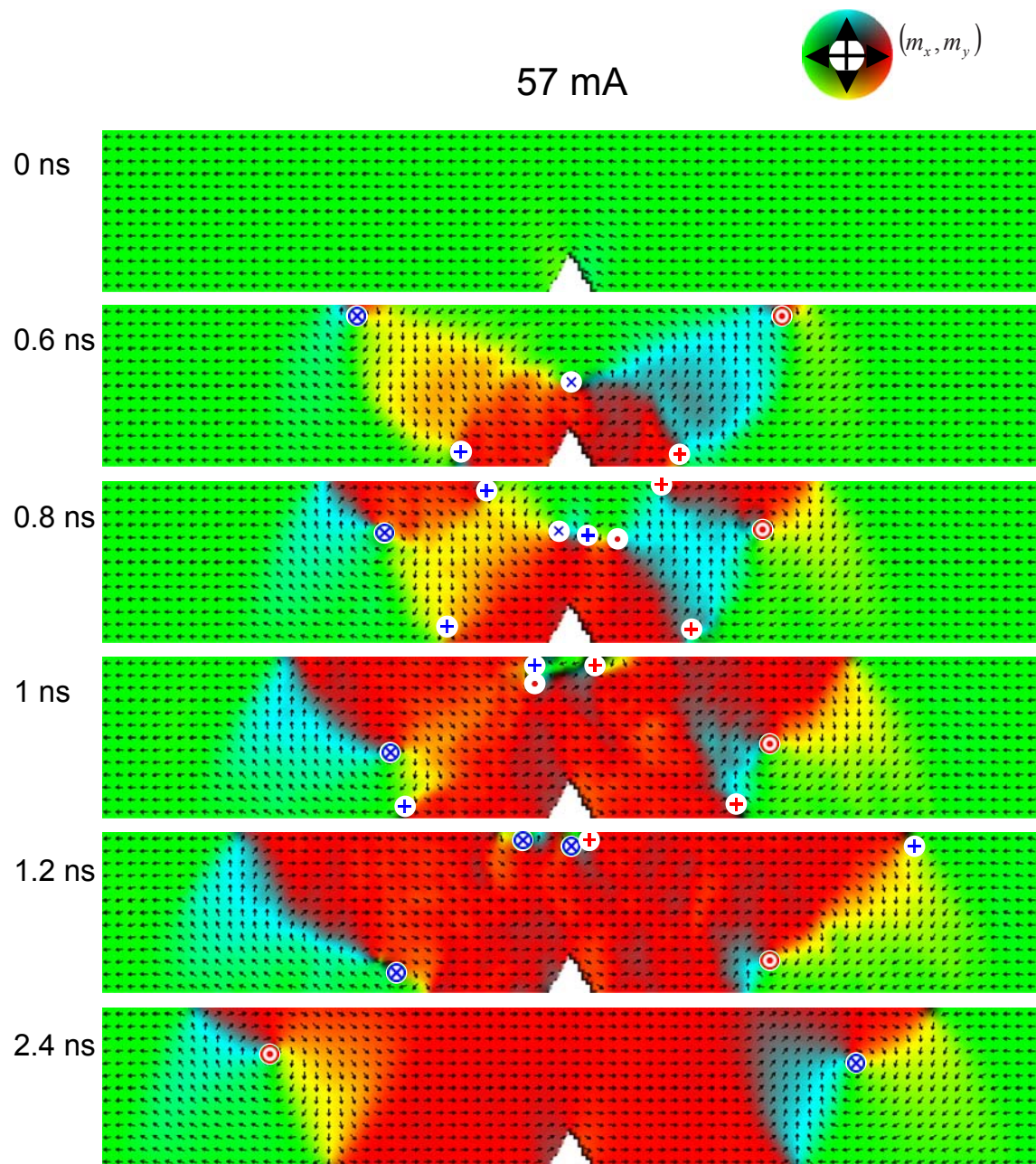
Figure S11 Blow up of the micromagnetic simulations from Fig. 2D showing the injection process for 57 mA of current applied to the injection line, resulting in the formation of CW DWs injected into the nanowire.

IV. Table showing the DW chirality injected as a function of injection current from LLG simulations

Note: 'ni' indicates no injection. "CCW/CW" corresponds to (first) counter-clockwise HH DW injected on the right and (second) clockwise TT domain wall injected on the left of the injection line.

The table above describes the chirality of the DWs obtained when an injection current is passed along the injection line placed perpendicular to the NW above it with the dimensions of the injection line and the NW as indicated. Just as an example, "Py 3000x200x20 500x200x90nm injection line" implies that the simulation was run for a NW that was 3000nm long, 200nm wide and 20nm thick and the injection line was 500nm wide along the length of the NW, 200nm wide (along the width of the NW) and 90nm thick. In every simulation, the wire is magnetized in the –x direction and the injection line is placed in the middle of the wire above the notch as shown in Fig. 2B. The notch is at the bottom edge of the NW unless otherwise mentioned in the table. Micromagnetic simulations were performed using LLG Micromagnetics software[10]. For the DW injection simulations, a Py wire with 3000nm long, 200nm wide, and 20nm thick was simulated. The cell size used in the simulation was set to 5x5x10nm^3. The saturation magnetization was taken to be 800emu/cm^3, exchange constant 1.050µerg/cm, and the anisotropy constant set at 1000erg/cm^3. A damping parameter of 0.01 was also used. (The Y-shaped junction as discussed in Fig. 3 was simulated as a 2000 nm long region, 1500 nm wide and 20 nm thick. The same cell size and parameters for Py as stated above were used for all the simulations.)

Every data point in the table corresponds to running the simulation with the appropriate dimensions and currents for 6-8 hours. 'ni' indicates no injection. "CCW/CW" corresponds to first counter clockwise HH DW injected on the right of the injection line and then clockwise TT domain wall injected on the left of the injection line, etc. The notch is placed on one edge and in some cases on both edges

of the NW with different sizes to see the effect on chirality control. As expected, the most dominant notch always acts as the nucleation site at minimum magnetic fields required for DW injection. Presence of the notch decreases the minimum current required for injection and the decrease scales with the size of the notch. At low currents just above the minimum current required for injection of DWs, the chirality is determined by the edge where the notch is placed. Beyond a certain value for injection current, the DW chirality switches to the opposite kind as the vortex cores that form on the edge opposite to the notch survive. Further increase again switches the chirality but the process is more stochastic as can be seen in the table.

Chirality control works for wider (200nm and 300nm) NWs but for 150nm wires, even when the nucleation process of the domain reversal is on expected lines, the chirality of the DWs may switch by going through a transient transverse DW in presence of large magnetic fields from the injection lines. As a consistency check, chirality control remains valid for injection lines of different widths. Most of the simulations were run for a 3ns long square-shaped electrical pulse but for consistency check we also ran a few simulations with the exact waveform with finite rise and fall times of the pulse as obtained from the Agilent 81110A pulser used in our experiments.

V. Topological defect in a Y-shaped junction in the saturated state

Although a bit counterintuitive, one can realize that there is a topological defect with n = -½ at one of the vertices at the node of the junction by either stretching one of the edges or bending the Y-shape into a T-shape. Topological theory guarantees that the winding number remains unchanged under smooth deformation of any physical system. The shapes obtained under such a deformation are called homotopic to each other. The three n = +½ defects exist at the tips of all these structures as discussed in Fig. 1 of the main text.
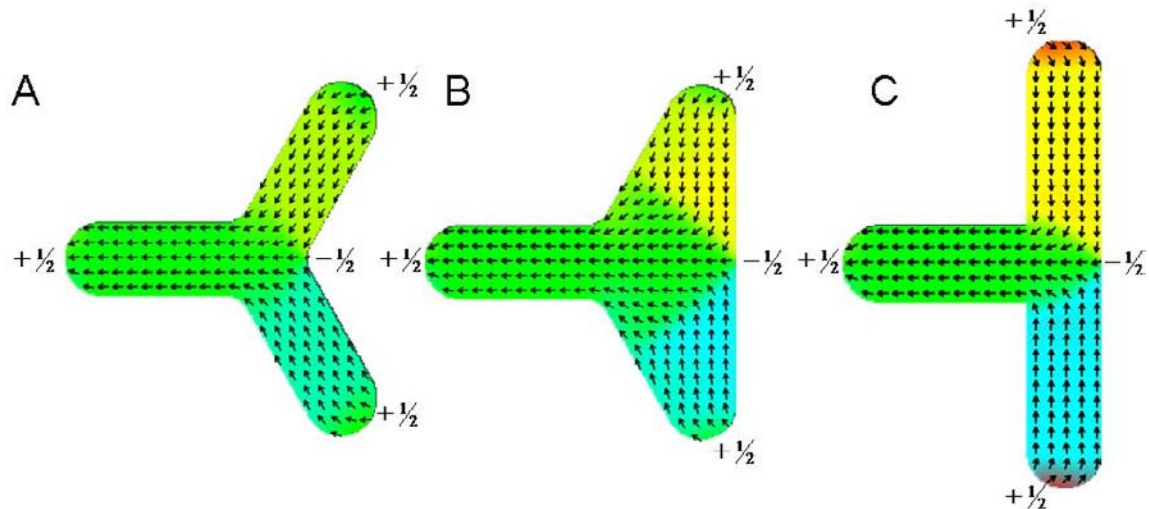

Figure S12 Y-shape can be deformed into B or C shapes to clearly visualize the n = -½ topological defect as indicated. All the three structures are homotopically equivalent to one another. These three structures are relaxed without any external field applied.

VI. Artificial Spin Ice Dirac String Formation

The remnant state after the honeycomb is fully saturated in the -x direction can be considered as a repeating set of two different types of nodes, represented as a and b in Fig. S13.
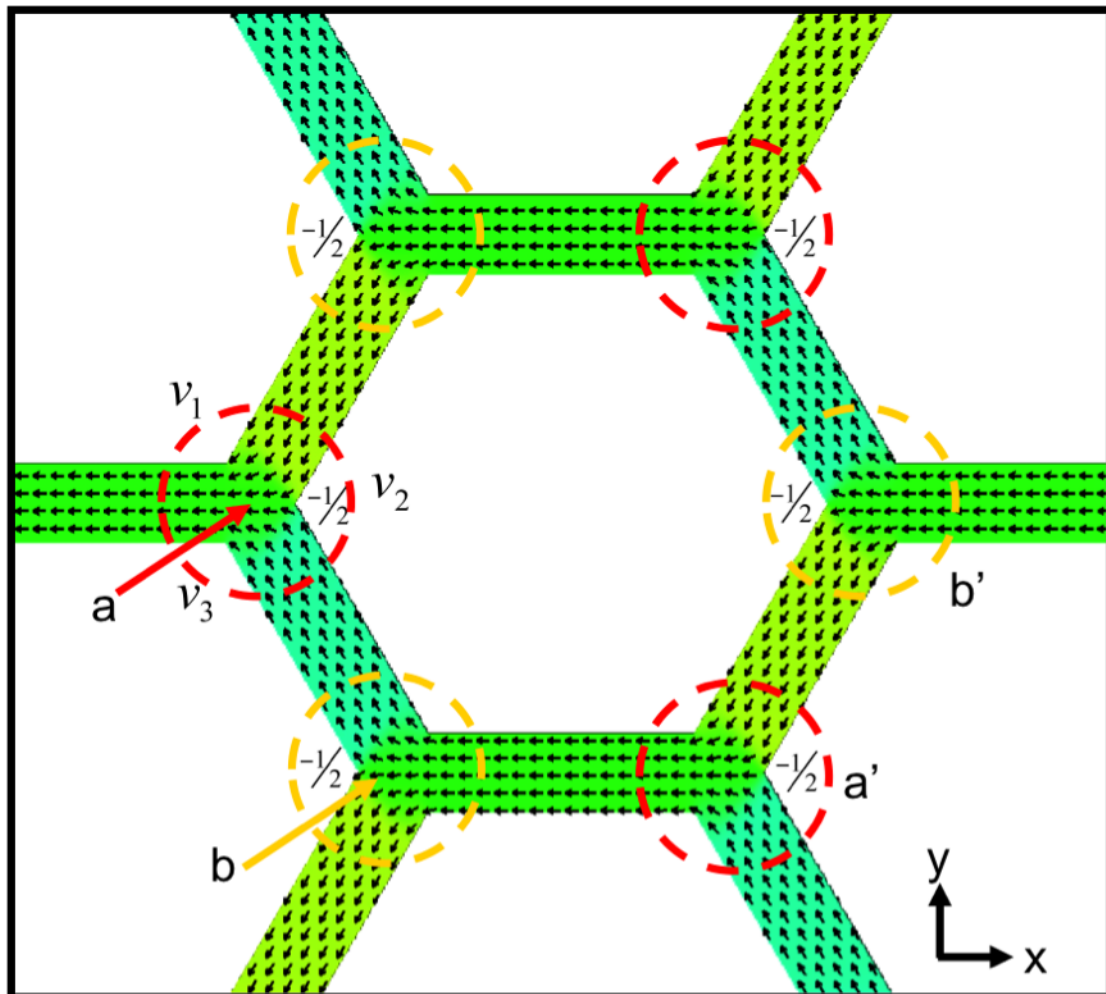

Figure S13 Remnant magnetization state of honeycomb network after being saturated in the -x direction. Denoted are the vertex positions where the n=-1/2 topological defect are positioned. The two types of nodes are denoted as a (red) and b (gold).

At the nodes represented by a, the n=-1/2 defect is at the vertex v_2 which is on the edge that is opposite to where the fractional topological defects of an incident DW (see Fig. 5A) would sit, namely the edges containing vertices v_1 and v_3. In contrast, at the node point b, the n=-1/2 defect of the network is on the same edge as where one of the fractional defects of an incident DW would be positioned (see Fig. 5B).

We will now consider the motion of the CCW DW into the honeycomb network (Fig. S14 A-C). The motion of the CCW DW to node a and into the branch between node a and b, is identical to what occurs in the branched junction, i.e., the DW gets sorted into one of the branches at node a depending upon its chirality (Figs. 3 and 4). However, upon entering into the lower branch, the leading fractional topological defect of the CCW DW is now on the same edge as the -1/2 defect at node b. In this case, the +1 topological bulk defect of the DW is attracted to both its own leading fractional topological as well as the -1/2 defect at node b (Fig. S14B), and thus annihilates, leaving behind only the trailing -1/2 topological defect at the opposing vertex of node b (Fig. S14C). It may be noted here that the outcome would remain the same even in the unlikely event of a CW DW traversing the branch between node a and node b. The +1 defect of the vortex DW will always annihilate with two of the -1/2 defects on the same edge of the network.
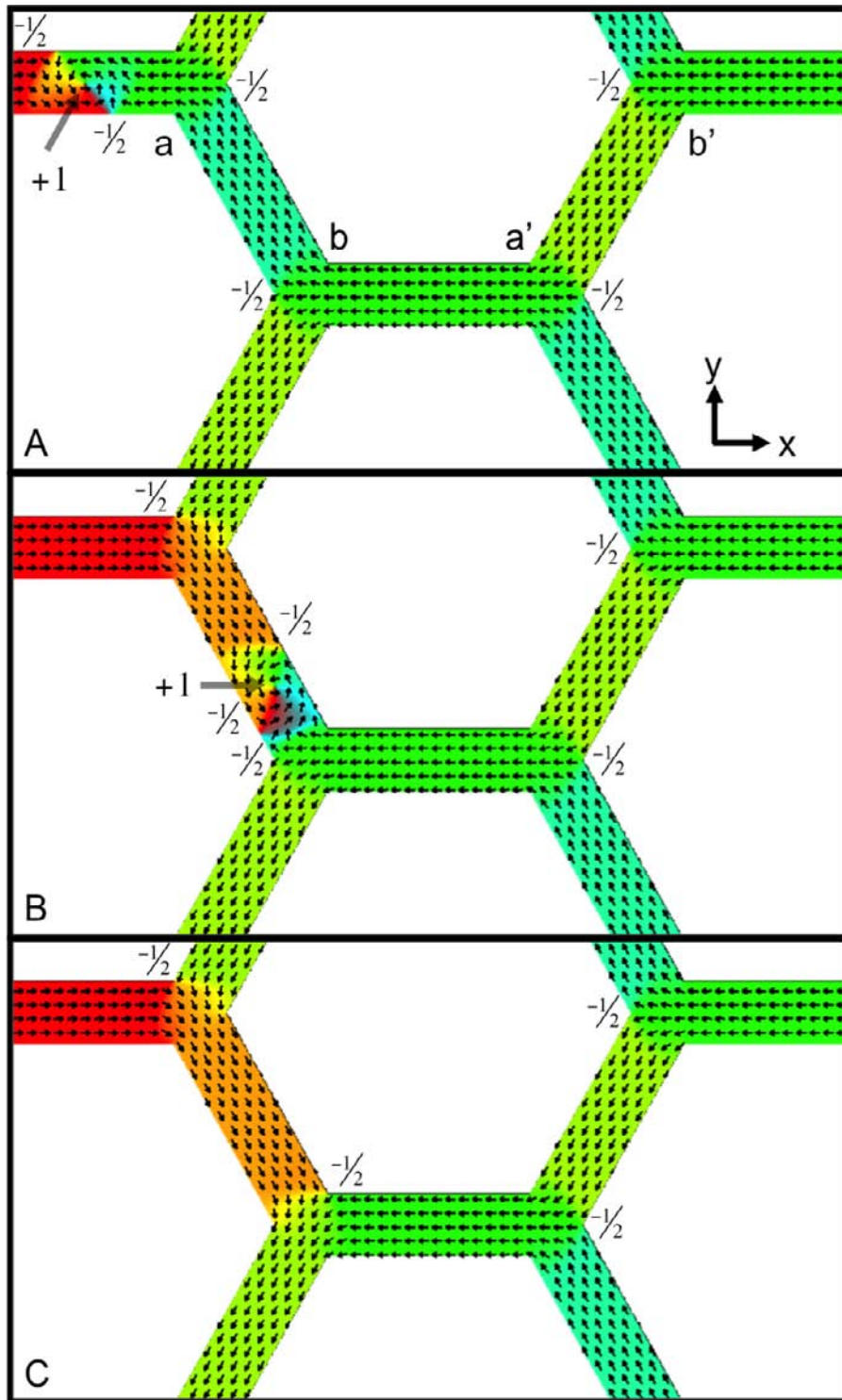
Figgure S14 (A) The CCW DW is introduced on the left most straight branch. **(B)** The CCW DW is sorted into the lower branch and enters into branch connecting nodes a and b **(C)** The remnant magnetization texture after the CCW DW has exited out from the branch linking nodes a and b.

In the presence of large enough magnetic fields, this -1/2 topological defect moves to the right (Fig. S15A), just as electrical charges move in the presence of electric fields. It should be noted that just the -1/2 defect doesn't constitute a DW. A +1/2 defect is required on the other edge to form a transverse DW; a combination of -1/2 defect on the opposite edge along with a +1 defect in the bulk is required for a vortex DW. Only a full-fledged DW can propagate freely in a network. This requirement leads to the introduction of +1/2 and -1/2 fractional topological defects on the lower edge of the same branch under large magnetic fields, as the preexisting -1/2 topological defect moves outward (Fig. S15A). The -1/2 topological defect on the top edge along with this leading +1/2 topological defect constitutes a CW transverse DW. Upon entering the node a', the transverse DW then goes towards the lower branch (Fig S15 B-C). Interestingly, we observe that in the case of a transverse DW, it is its +1/2 topological defect that determines the trajectory of the DW through a branched junction as it forms a DW with the pre-existing nodal -1/2 defect. This is different from a vortex DW where its leading -1/2 defect decides the branch selection. It can now be clearly seen that subsequent chain of repetitive events at nodes of type a and b would lead to the formation of a staircase Dirac string (Fig. 5F inset).
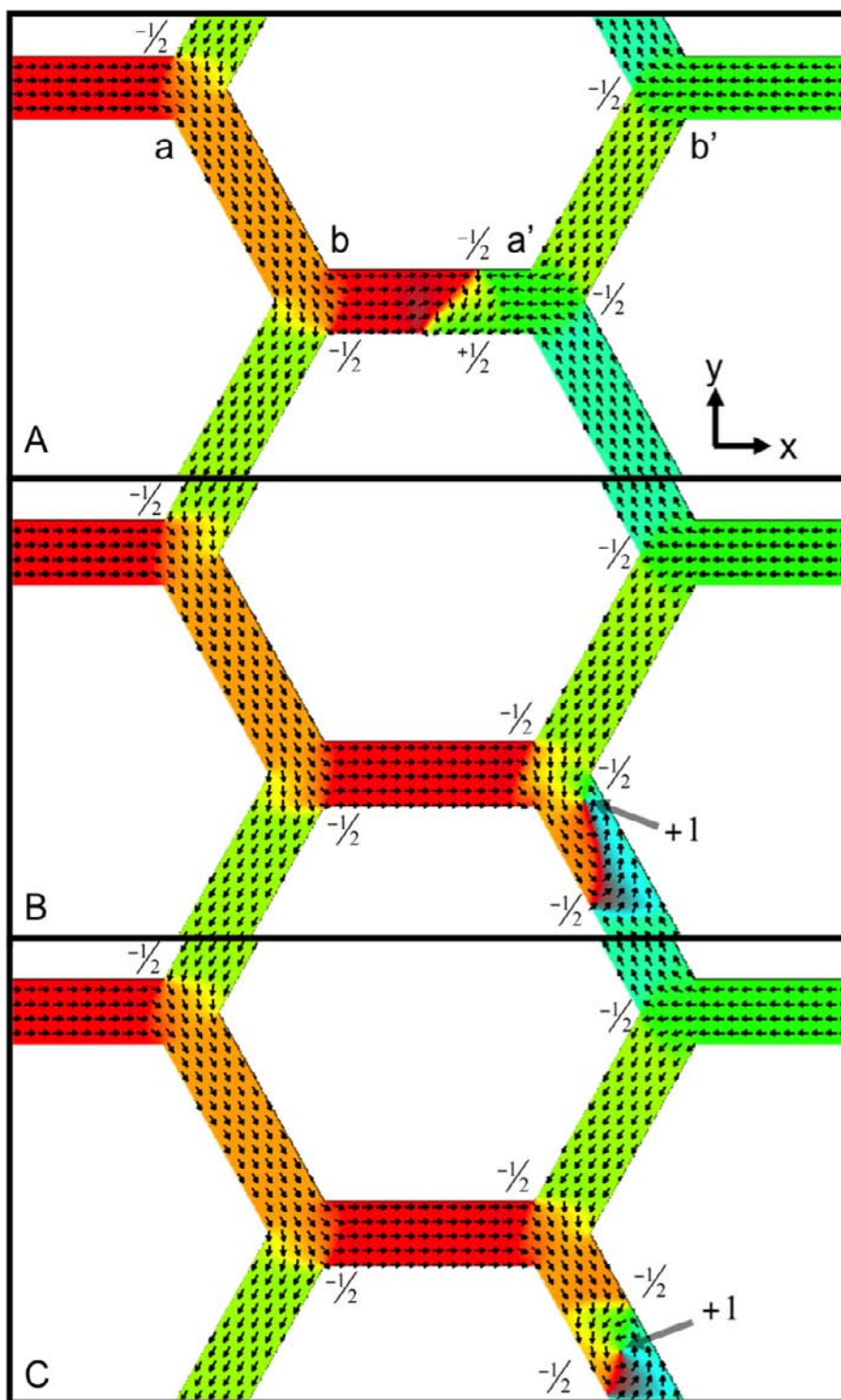
Figure S15 (A-C) Micromagnetic simulation showing the formation of a staircase Dirac string.

There is a second possibility during the creation of +1/2 and -1/2 defects in the presence of large magnetic fields discussed earlier in Fig. S15A. Instead of a CW transverse DW, a CW vortex DW may form in the branch connecting nodes b and a' when the +1/2 topological defect of the transverse DW switches into a -1/2 defect by emitting a +1 topological defect in the bulk (Fig. S16A). This is more likely for the wider NWs which favor vortex DWs over transverse DWs. We know from Figs. 3&4 that a CW vortex DW after reaching node a' would prefer to move into the upper branch (Fig. S16B-C). Subsequent chain of repetitive events at nodes of type a and b would lead to the formation an armchair Dirac string (Fig. 5F' inset).

A combination of staircase and armchair Dirac strings is also possible depending upon which type of DW is getting to the nodes of type a in the artificial ice network, where branch selection takes place. Regardless of these possibilities, the one dimensionality of the switching of the artificial spin ice network is a consequence of the fractional topological defects of the DWs determining their trajectories.
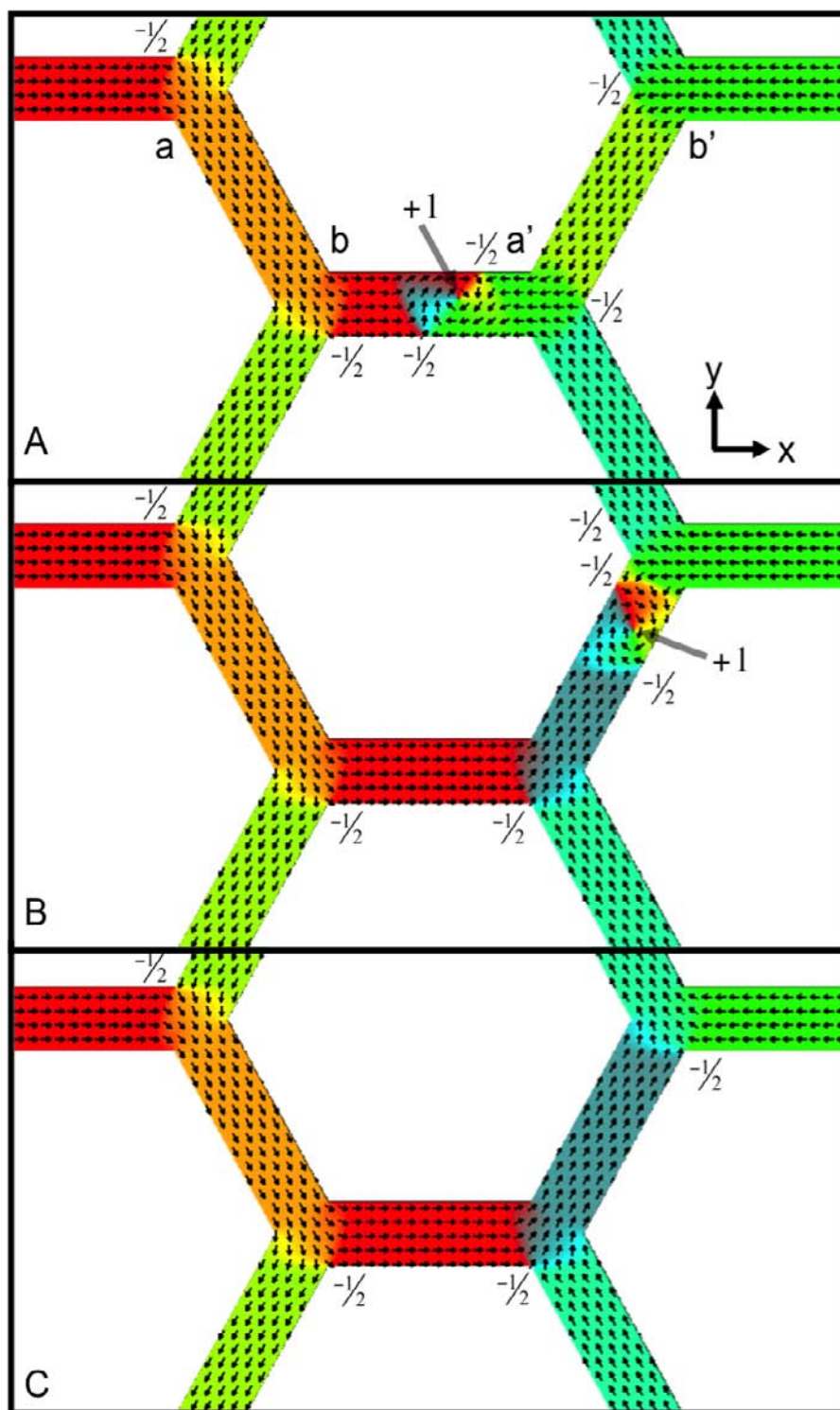
Figure S16 (A-C) Micromagnetic simulation showing the formation of an armchair Dirac string.

References

1   Mermin, N. D. The topological theory of defects in ordered media. *Reviews of Modern Physics* **51**, 591-648 (1979).

2   Chaikin, P. M. & Lubensky, T. C. *Principles of Condensed Matter Physics.* (Cambridge University Press, 2000).

3   Tchernyshyov, O. & Chern, G.-W. Fractional Vortices and Composite Domain Walls in Flat Nanomagnets. *Physical Review Letters* **95**, 197204 (2005).

4   Schryer, N. L. & Walker, L. R. The motion of 180[degree] domain walls in uniform dc magnetic fields. *Journal of Applied Physics* **45**, 5406-5421 (1974).

5   McMichael, R. D. & Donahue, M. J. Head to head domain wall structures in thin magnetic strips. *IEEE Transactions on Magnetics* **33**, 4167-4169 (1997).

6   Thiele, A. A. Steady-State Motion of Magnetic Domains. *Physical Review Letters* **30**, 230-233 (1973).

7   Tretiakov, O. A., Clarke, D., Chern, G.-W., Bazaliy, Y. B. & Tchernyshyov, O. Dynamics of Domain Walls in Magnetic Nanostrips. *Physical Review Letters* **100**, 127204 (2008).

8   Thiaville, A. & Nakatani, Y. in *Spin Dynamics in Confined Magnetic Structures III* Vol. 101 *Topics in Applied Physics*   161-205 (2006).

9   Tretiakov, O. A. & Tchernyshyov, O. Vortices in thin ferromagnetic films and the skyrmion number. *Phys Rev B* **75**, 012408 (2007).

10   LLG Micromagnetics   Simulator <http://llgmicro.home.mindspring.com> (1997).